Three-dimensional ambient noise modeling in a submarine canyon

David R. Barclay, and Ying-Tsong Lin

Citation: The Journal of the Acoustical Society of America **146**, 1956 (2019); doi: 10.1121/1.5125589
View online: https://doi.org/10.1121/1.5125589
View Table of Contents: https://asa.scitation.org/toc/jas/146/3
Published by the Acoustical Society of America

Three-dimensional ambient noise modeling in a submarine canyon

David R. Barclay[1,a)] and Ying-Tsong Lin[2]
[1]*Department of Oceanography, Dalhousie University, 1355 Oxford Street, Halifax, Nova Scotia, B3H 4R2, Canada*
[2]*Applied Ocean Physics and Engineering Department, Woods Hole Oceanographic Institution, 266 Woods Hole Road, Woods Hole, Massachusetts 02543-1050, USA*

(Received 6 September 2018; revised 21 March 2019; accepted 23 March 2019; published online 1 October 2019)

A quasi-analytical three-dimensional (3D) normal mode model for longitudinally invariant environments can be used to compute vertical noise coherence in idealized ocean environments. An examination of the cross modal amplitudes in the modal decomposition of the noise cross-spectral density shows that the computation can be simplified, without loss of fidelity, by modifying the vertical and horizontal mode sums to exclude non-identical mode numbers. In the special case of a Gaussian canyon, the across-canyon variation of the vertical wave number associated with each mode allows a set of horizontally trapped modes to be generated. Full 3D and Nx2D parabolic equation sound propagation models can also be used to calculate vertical noise coherence and horizontal directionality. Intercomparison of these models in idealized and realistic canyon environments highlights the focusing effect of the bathymetry on the noise field. The absolute vertical noise coherence increases, while the zero-crossings of the real component of the coherence are displaced in frequency when out-of-plane propagation is accounted for. © *2019 Acoustical Society of America*.
https://doi.org/10.1121/1.5125589

[JAC] Pages: 1956–1967

I. INTRODUCTION

Accurate models of the spatial coherence of ambient noise can be used to improve detection of deterministic signals by informing array design and signal processing algorithms. In deep water environments, simple models of surface generated noise have been experimentally verified to be accurate over a large range of depths (Cron and Sherman, 1962; Barclay and Buckingham, 2013), while shallow water noise fields have been modeled in a stratified range independent ocean using modal (Kuperman and Ingenito, 1980) and wave number integral techniques (Deane *et al.*, 1997). Parabolic equation (PE) propagation models have been used in a range independent two-dimensional (2D) ocean to predict the vertical noise directionality (Carey *et al.*, 1990). Extending spatial coherence noise models to three dimensions has been made using the adiabatic normal mode approximation (neglecting mode coupling) over large domains of hundreds of kilometers of deep ocean to investigate downslope contributions to the noise field's directionality (Perkins *et al.*, 1993). These models can be used to predict the second-order statistics for noise generated by bubbles due to breaking and spilling waves at the sea surface, a nearly ubiquitous source of ambient noise in the ocean over the band from 100 Hz to tens of kHz.

However, three-dimensional (3D) propagation effects can dramatically change the transmission characteristics of sound in shallow water over smaller scales, such as near a submarine canyon (Lin *et al.*, 2015), shelf break front (Lin and Lynch, 2012), set of seafloor scours (Ballard *et al.*, 2012), shallow banks or shoal (Sagers *et al.*, 2014), or shallow water wedge (Glegg and Yoon, 1990; Heaney and Murray, 2009). In these cases and near other complex shallow water bathymetries, the ambient noise level statistics and horizontal and vertical coherences (directionality) will also exhibit 3D characteristics, such as increased noise intensity due to horizontal focusing, or perturbed horizontal noise directionality due to out-of-plane propagation. In this work, the 3D features of the ambient noise field are demonstrated for the particular cases of an idealized and realistic submarine canyon. A quasi-analytical normal mode model and computational PE ambient noise model are used to predict the power and spatial properties of the noise field and provide orientation specific estimates of the coherence.

Ocean ambient noise is increasingly being used in acoustical oceanographic inversion problems, such as the estimate of geoacoustic properties, wind speeds, and rainfall rates, often under the assumption of simplified bathymetry. In cases of empirical wind-noise and rainfall rate-noise relationships, the shallow water propagation environment is too complex and does not allow meaningful observations to be made (Vagle *et al.*, 1990). Passive acoustic inversions of seabed acoustic properties have shown that the compressional and shear wave speeds and attenuation, sediment density, and presence of sub-bottom layering can all alter the vertical noise coherence (Deane *et al.*, 1997; Carbone *et al.*, 1998; Siderius *et al.*, 2006). The water column sound speed profile and variations in local sound speed also have an effect on the vertical and horizontal noise coherences (Buckingham, 1994; Barclay and Buckingham, 2013). Other parameters known to alter underwater sound transmission, such as internal waves

a)Electronic mail: dbarclay@dal.ca

(Lin *et al.*, 2013b) and bottom roughness (Perkins and Thorsos, 2007), may also have observable effects on the noise intensity and coherence. This study shows the feasibility of using a 3D PE model with idealized boundaries and isovelocity sound speed profiles to more carefully understand the bathymetric effects on the surface wave generated ambient noise intensity and coherence, including the effects of horizontal refraction and reflection. It is demonstrated that such effects are similar in magnitude to the other environmental mechanisms discussed above under special circumstances, for example, the vertical coherence in the overlapping ship noise and ambient noise frequency band (75–500 Hz) in a submarine or shelf break canyon.

In this paper we present three methods for modeling ambient noise in a longitudinally invariant environment, using an infinitely long Gaussian canyon as a demonstration. In Sec. II A a semi-analytical model is developed using vertical and horizontal normal mode decompositions for the arbitrary longitudinally invariant case and extended to a Gaussian canyon example in Sec. II B. The reciprocal Nx2D PE and cylindrical PE noise models are discussed in Sec. II C. The results from the three methods applied to a Gaussian canyon example are presented and discussed in Sec. III. Last, Sec. IV shows the results for the PE computational noise models applied to a realistic shelf break canyon environment.

II. METHODS

A. 3D normal mode solution in a longitudinally invariant waveguide

The coordinate system considered here is a 3D Cartesian space, while the general idealized model geometry contains a pressure release sea surface, isovelocity water column, homogenous seabed, and a topography $H(y)$, which is range dependent in the y coordinate, but range independent in the x coordinate, or longitudinally invariant. An infinitely long Gaussian canyon discussed in Sec. II B is a particular case of this more general model geometry.

We are seeking a solution to the wave equation that describes the propagation between an arbitrarily placed source and receiver with modal components in the vertical and y directions and a complete solution in the x direction. We begin with the spectral representation of the acoustic wave equation with a point source placed at (x_0,y_0,z_0),

$$\nabla^2 p + k^2 p = -4\pi\delta(x-x_0)\delta(y-y_0)\delta(z-z_0), \tag{1}$$

where the wave number $k=\omega/c$, ω is the angular frequency, c is the sound speed, p is the acoustic pressure, and $\delta(\cdot)$ is the Dirac delta function.

The solution to Eq. (1) can be found in the following form using the adiabatic normal-mode approach:

$$p(x,y,z) = \sum_m \sum_n A_{mn}(y,z)\chi_{mn}(x), \tag{2}$$

where $A_{mn}(y,z)$ is the 2D mode of order m and n determined from the eigenvalue problem with boundary conditions on the cross section of the waveguide,

$$\frac{\partial^2 A_{mn}}{\partial y^2} + \frac{\partial^2 A_{mn}}{\partial z^2} + \left(k^2 - k_{x,mn}^2\right)A_{mn} = 0, \tag{3}$$

where $k_{x,mn}$ is the eigenvalue of mode A_{mn}, and the mode coupling terms have been neglected. In Eq. (2), the longitudinal component of the solution $\chi_{mn}(x)$ is governed by the one-dimensional (1D) wave equation with the adiabatic normal-mode approximation,

$$\frac{d^2\chi_{mn}}{dx^2} + k_{x,mn}^2\chi_{mn} = -4\pi\delta(x-x_0)A_{mn}(y_0,z_0), \tag{4}$$

where the closure property of normal modes is exploited to expand the Dirac delta function, and the eigenvalue $k_{x,mn}$ is, in fact, the horizontal wave number of mode A_{mn}. The solution to Eq. (3) can be readily found to be

$$\chi_{mn}(x) = 2\pi i A_{mn}(y_0,z_0)\frac{e^{\pm ik_{x,mn}|x-x_0|}}{k_{x,mn}}. \tag{5}$$

If we approximate the cross section of the waveguide to be a series of range independent vertical patches, there will be a set of 1D vertical modes configuring the local sound pressure structure within each vertical patch and determined from the next eigenvalue problem subject to the local boundary conditions

$$\left\{\frac{d^2}{dz^2}\phi_m + \left[k^2 - \zeta_m^2\right]\phi_m\right\}\Big|_{y'} = 0, \tag{6}$$

where y' indicates the location of the patches, and ζ_m is the eigenvalue of mode ϕ_m and gives the vertical wave number $k_{z,m}$ from the equation

$$k_{z,m}^2 = k^2 - \zeta_m^2. \tag{7}$$

If we further assume the vertical patches to be infinitesimal and neglect the horizontal gradient of the vertical modes across the patches (neglect the mode coupling in the y direction), the 2D mode function $A_{mn}(y,z)$ can be decomposed in the following way:

$$A_{mn}(y,z) = \psi_{mn}(y)\phi_m(y,z), \tag{8}$$

where the vertical mode ϕ_m is practically 2D because the vertical patches are considered to be infinitesimal. Substituting A_{mn} in Eq. (3) with the decomposition yields the equation to determine $\psi_{mn}(y)$

$$\frac{d^2\psi_{mn}}{dy^2} + \left[\zeta_m^2(y) - k_{x,mn}^2\right]\psi_{mn} = 0. \tag{9}$$

As the last step of the normal mode approach, combining the by-parts solutions to Eqs. (4), (6), and (9) gives an expression for the complex pressure at a point $\mathbf{x}=(x,y,z)$ due to a source at $\mathbf{x}_0=(x_0,y_0,z_0)$ in the following double infinite sum over mode numbers m and n:

$$p(x,y,z) = i2\pi \sum_m \sum_n \psi_{mn}(y_0)\phi_m(y_0,z_0) \times \psi_{mn}(y)\phi_m(y,z)\frac{e^{\pm ik_{x,mn}|x-x_0|}}{k_{x,mn}}. \quad (10)$$

The adiabatic assumption has been used to derive Eq. (10). From Eq. (10) it can be seen that for each vertical mode m, the equation has a completely independent set of horizontal modes, indexed in both m and n. This normal mode solution can then be used to calculate the ambient noise field due to breaking waves by assuming the noise sources are placed uniformly on an infinite plane parallel to the ocean's surface and at a depth z_0.

To calculate the spatial cross-spectral density of a random noise field between two receivers placed at $\mathbf{x}_1 = (x_1,y_1,z_1)$ and $\mathbf{x}_2 = (x_2,y_2,z_2)$ at a single frequency, S_{12}, we must integrate over the infinite source distribution, giving

$$S_{12}(\mathbf{x}_1,\mathbf{x}_2) = \int\int_{-\infty}^{\infty} \langle|\sigma(x_0,y_0)|^2\rangle p_1 p_2^* \, dx_0 \, dy_0, \quad (11)$$

where $\langle|\sigma(x_0,y_0)|^2\rangle$ is the ensemble average of the noise source strength at $\mathbf{x}_0 = (x_0,y_0)$, and p_1 and p_2 are the Green's functions from $\mathbf{x}_0$ to $\mathbf{x}_1$ and $\mathbf{x}_2$, respectively. In the case of wind driven noise, the value of $\langle|\sigma(x_0,y_0)|^2\rangle$ is taken to be constant everywhere.

Inserting Eq. (10) into Eq. (11) gives the full expression as four infinite sums and two infinite integrals over products of the mode functions and the free-space solution in the longitudinally invariant direction x,

$$\begin{aligned} S_{12} = 2\pi i \sum_m \sum_n \sum_{m'} \sum_{n'} & \psi_{mn}(y_1)\,\phi_m(y_1,z_1) \\ & \times \psi_{m'n'}{}^*(y_2)\,\phi_{m'}{}^*(y_2,z_2) \\ & \times \int_{-\infty}^{\infty} \langle|\sigma(x_0,y_0)|^2\rangle \psi_{mn}(y_0)\psi_{m'n'}{}^*(y_0) \\ & \times \phi_m(z_0;y_0)\phi_{m'}{}^*(z_0;y_0)\,dy_0 \\ & \times \int_{-\infty}^{\infty} \frac{e^{-ik_{x,mn}|x_1-x_0|}}{k_{x,mn}} \left[\frac{e^{-ik_{x,m'n'}|x_2-x_0|}}{k_{x,m'n'}}\right]^* dx_0. \end{aligned} \quad (12)$$

The primed indexes in m and n have been introduced to distinguish the conjugated modes of p_2* from the unconjugated modes of p_1. Here, the sign convention of the exponential term is selected to be negative. To calculate the power spectral density, we can simply substitute p_1* in the place of p_2*.

The integral in x_0 given in Eq. (12) can be evaluated within the sums and has an analytical solution given by

$$\begin{aligned} & \int_{-\infty}^{\infty} \frac{e^{-ik_{x,mn}|x_1-x_0|}}{k_{x,mn}} \left[\frac{e^{-ik_{x,m'n'}|x_2-x_0|}}{k_{x,m'n'}}\right]^* dx_0 \\ & = \frac{2i\{k_{x,mn}e^{-2\Delta i k^*_{x,m'n'}} + k^*_{x,m'n'}e^{2\Delta i k_{x,mn}}\}}{k^*_{x,m'n'}k_{x,mn}(k_{x,mn}+k^*_{x,m'n'})(k_{x,mn}-k^*_{x,m'n'})}, \end{aligned} \quad (13)$$

where the separation between the two receivers in the x direction is written as

$$\Delta = |x_2 - x_1|. \quad (14)$$

For each term in the four infinite sums, the solution to the integral shown in Eq. (13) gives a cross modal amplitude indexed by m, n, m', and n'. The properties of this function determine which products of modes will generate the dominant terms over this four-dimensional summation. From the expression, it is evident that in instances where the difference between the longitudinal wave numbers, $k_{x,mn} - k^*_{x,m'n'}$ is minimized, the cross modal amplitude will be a maximum.

It is also important to note that $k_{x,mn}$ will be complex for the evanescent modes or in the case where k is complex due to medium attenuation. In an ideal case where $k_{x,mn}$ is real and when $m' = m$ and $n' = n$, Eq. (13) will have identical longitudinal wave numbers and the quadruple sum will be infinite—an intuitive result, as we are integrating over an infinite sheet of noise sources. Due to the very small sound absorption in seawater, this is never the case in reality, and thus the cross modal amplitudes must always be finite, and the noise field in the ocean must always have a finite value despite the contributions from an infinite number of sources.

So long as ϕ_m, the vertical mode shapes, may be computed, the generalized situation of an arbitrarily complex water column sound speed profile, seabed acoustic properties, and bottom layering can be considered in calculating the cross-spectral density S_{12}. This can be accomplished using numerical techniques (Westwood *et al.*, 1996). Here, the idealized case of a fluid seabed with an overlying isovelocity sound speed profile is considered as a simple example to provide some insight into the normal mode solution equation (12). The vertical modes can be found using the effective depth approximation (Weston, 1960) for a fast fluid seabed, where the bottom is replaced by a pressure release boundary placed at a distance ΔH beneath the true interface depth such that the geometrical phase change experienced by a ray (equivalent to a given mode) is approximately equal to the true phase change (Buckingham, 1979). For a fast, lossless fluid bottom, ΔH is given by

$$\Delta H = \frac{1}{b_{12}kH\sin(\alpha_c)}, \quad (15)$$

where b_{12} is the density ratio, and α_c is the critical grazing angle of the bottom. The advantage of this approximation is that the vertical modes have the following sinusoidal solution in the water column:

$$\phi_m = \sqrt{\frac{2}{H_e}}\sin(k_{z,m}z), \quad 0 < z < H, \quad (16)$$

where $H_e = H + \Delta H$, and the vertical wave numbers are given by

$$k_{z,m} = m\frac{\pi}{H_e}. \quad (17)$$

As the bathymetry H is a function of y, so the mode functions and modal wave numbers vary in y. With Eqs. (16) and (17), we can also obtain an asymptotic formulation using the

first-order Taylor expansion for the modal excitation term in Eq. (12), i.e.,

$$\phi_m(y_0, z_0) \cong \sqrt{\frac{2}{H_e(y_0)}} m \frac{\pi}{H_e(y_0)} z_0. \tag{18}$$

Substituting Eqs. (16)–(18) in the normal mode solution, Eq. (12), and assuming homogeneous noise strength, we can reach the following equation for spatial cross-spectral density:

$$\begin{aligned} S_{12} = \langle |\sigma|^2 \rangle \sum_m \sum_n \sum_{m'} \sum_{n'} & mm' \psi_{mn}(y_1)\, \psi_{m'n'}{}^*(y_2) \\ & \times \phi_m(y_1, z_1) \phi_{m'}{}^*(y_2, z_2) \\ & \times 2\pi^2 z_0^2 \int_{-\infty}^{\infty} H_e{}^{-3}(y_0) \psi_{mn}(y_0) \psi_{m'n'}{}^*(y_0)\, dy_0 \\ & \times \frac{2i\left\{k_{x,mn} e^{-2\Delta i k^*_{x,m'n'}} + k^*_{x,m'n'} e^{2\Delta i k_{x,mn}}\right\}}{k^*_{x,m'n'} k_{x,mn} (k_{x,mn} + k^*_{x,m'n'})(k_{x,mn} - k^*_{x,m'n'})}. \end{aligned} \tag{19}$$

Since the bathymetry H is a function of y_0, the orthogonality of modes may not be used to reduce the integral term over y_0.

However, the relative values of the cross modal amplitudes are useful for truncating the series solution to certain mode numbers m and n, and therefore greatly reducing the computational complexity of calculating the cross-spectral density. Figure 1 shows the four-dimensional matrix of depth independent cross modal amplitudes of the noise field at 100 Hz for two sensors with a half-wavelength spacing in a 500 m deep waveguide, on a base 10 log scale for (n, n', m, $m'<10$) by recasting the dimensions into two. With the inclusion of seawater absorption, 10^{-3} at 100 Hz, the terms where $m = m'$ and $n = n'$ remain finite but are significantly larger than the others suggest that the quadruple sum may be greatly simplified with minimal loss of fidelity in the modal solution.

This disparity between identical and cross modes is accentuated in the vertical relative to the horizontal, particularly for low order modes. Low order vertical modes, adjacent horizontal cross modal amplitudes are −5 dB below the peak $n = n'$ amplitudes, much larger than those across vertical modes. For higher order vertical modes, neither the horizontal nor vertical cross modal amplitudes are significant.

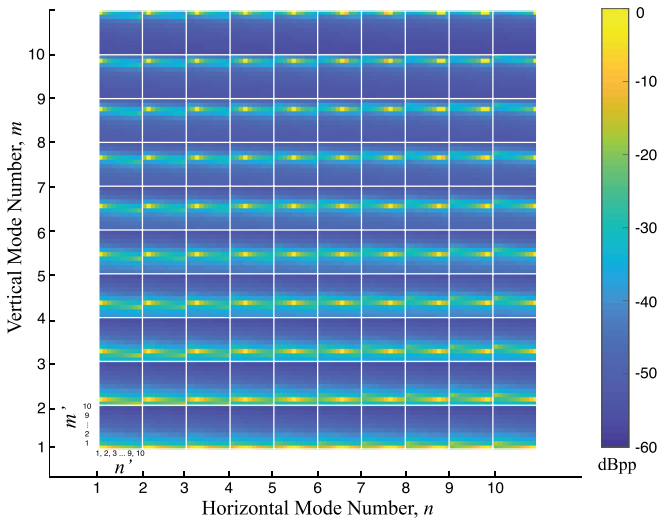

FIG. 1. (Color online) Four-dimensional cross modal amplitudes for the horizontal and vertical mode decompositions of the cross-spectral density of surface generated noise in a generalized longitudinally invariant environment.

In the case where the receivers are aligned within the y-plane, in other words, when $\Delta = 0$ in Eq. (13), the expression for the cross modal amplitudes simplifies even further to

$$\frac{2i}{k^*_{x,m'n'} k_{x,mn} (k_{x,mn} - k^*_{x,m'n'})}, \tag{20}$$

showing clearly that the difference in longitudinal wave numbers drives relative significance of the cross modal amplitudes. In this case the depth independent cross modal amplitudes for two sensors with an arbitrary spacing on the yz-plane are significantly greater when $n = n'$ and $m = m'$, suggesting that the quadruple sum may again be simplified and truncated.

Techniques for further generalizing this model to incorporate a depth dependent sound speed profile in the water column, as well as depth dependent viscoelastic seabed, are available and will give more realistic vertical mode shapes and perturbed vertical mode numbers, altering the horizontal modes shapes and mode numbers as well. In Sec. II B, the normal mode approach is applied to the case of an idealized, longitudinal invariant canyon model, and used to compute the noise cross-spectral density between two receiver points.

B. Normal mode solution in a Gaussian canyon

The cross modal amplitudes and an expression for the cross-spectral density for two arbitrarily space receivers in a generalized longitudinally invariant ocean environment were derived. The Gaussian canyon model is a special case of such a problem, where

$$H(y) = Ce^{-(y/C)^2} + B, \tag{21}$$

and the maximum depth of the canyon is given by C while the minimum water depth at the canyon's shoulders is given by B.

In the idealized case considered in this paper, the vertical modes and vertical wave number are given by Eqs. (16) and (17), where the wave number now has an explicit across-canyon functionality.

This allows us to write the horizontal across-canyon component of the wave equation in a closed form by combining Eqs. (9), (17), and (21),

$$\frac{d^2\psi_{mn}}{dy^2} + \left[k^2 - m^2 \frac{\pi^2}{\left(Ce^{-(y/C)^2} + B\right)^2} - k^2_{x,mn}\right] \psi_{mn} = 0, \tag{22}$$

subject to the following simplified boundary condition:

$$\lim_{y \to \pm\infty} \psi_{mn} = 0. \tag{23}$$

Note that it is straightforward to employ the more general Sommerfeld radiation boundary condition to include oscillatory

solutions for ψ_{mn}, but without loss of generality, especially for trapped modes, we choose this simplified boundary condition for easier discussion.

The existence of an analytical solution to such an equation is not immediately obvious. The method of finite difference is appropriate for finding the across-canyon horizontal mode shapes and mode numbers for each vertical mode. To do so, the across-canyon dimension must become finite over the interval $-D < y < D$, where D is large enough to extend beyond the domain where the Gaussian changes rapidly. With this satisfied, the approximation to the radiation condition can be written as

$$\psi_{\pm D,mn} = 0. \tag{24}$$

The radiation condition requires that the across-canyon horizontal wave number be purely imaginary at $\pm D$, the boundaries of the domain, and the horizontal across-canyon mode number $k_{y,mn}(y)$ are calculated from the characteristic equation. Lastly, the normalization condition,

$$\int_{-\infty}^{\infty} |\psi_{mn}(y)|^2 dy = 1, \tag{25}$$

is applied, providing the complete solution to Eq. (22).

C. Nx2D and cylindrical 3D PE models in a Gaussian canyon

1. Reciprocal PE

In order to consider more complex and realistic canyon bathymetries, bottom types, bottom roughness, and spatially variable sound speed profiles, we introduce the use of a PE sound propagation model for the simulation of noise. In this case, the PE model will exploit the reciprocity nature of the wave equation by modeling the receiver as a computational source at $\mathbf{x}_1$ and computing the complex pressure field $p(\omega,x_i,y_j,z_k)$ everywhere in the domain, where the indexed spatial variables represent the discrete Cartesian grid, and ω is a single angular frequency. Then, by invoking reciprocity, the noise power $S_{11}(\omega)$ due to a quasi-infinite sheet of noise sources placed just below the surface at a depth z', can be obtained through the discretized and simplified version of Eq. (11),

$$S_{11}(\omega) = \sum_{i=-\infty}^{\infty} \sum_{j=-\infty}^{\infty} \langle |\sigma(x_i,y_j)|^2 \rangle |p(\omega,x_i,y_j,z')|^2 \Delta x_i \Delta y_j, \tag{26}$$

where, in practice, the limits of the summation indices i and j will be finite and $\Delta x_i \Delta y_j$ represent the particular case of the Cartesian element of area over which the noise sources have been averaged.

The cross-spectral density can be computed by running a second instance of the model, this time with the source (reciprocal receiver) placed at $\mathbf{x}_2$, and by combining the results through the discrete version of Eq. (11),

$$S_{12}(\omega) = \sum_{i=-\infty}^{\infty} \sum_{j=-\infty}^{\infty} \langle |\sigma(x_i,y_j)|^2 \rangle p_1(\omega,x_i,y_j,z') \times p_2{}^*(\omega,x_i,y_j,z') \Delta x_i \Delta y_j. \tag{27}$$

This reciprocal method of noise is discussed in detail by Jensen and Carey in their texts on computational acoustics and ocean ambient noise, respectively (Jensen, 1994; Carey and Evans, 2011). In Carey's seminal paper on PE noise modeling on a vertical array, an additive noise marching scheme is used in lieu, where at each range step in the algorithm's marching routine, a noise source is added just below the sea surface with a randomly chosen phase (Carey *et al.*, 1990). This increases computational efficiency as the resultant pressure field at the final marching step contains contributions from all noise sources, thus provides the modeled noise power at every depth. However, as the additive superposition of noise sources is coherent with the marching, a large (~20–30) number of model realizations must be executed to achieve a stable estimate of the noise field (Dyer, 1973). In our case, as we are only dealing with two receivers, the reciprocal method is less costly from a computational perspective. In order to reproduce the coherence curve between two arbitrarily spaced sensors, the code must be run once at each desired frequency and sensor location combination. This method is benchmarked below against the known solution in a Pekeris waveguide (Deane *et al.*, 1997).

The complex pressure field computed at z' for a source at an arbitrary location $\mathbf{x_i}$ can be plotted as a transmission loss, which, in reciprocity, describes the surface receive sensitivity for a receiver placed at $\mathbf{x_i}$. The surface receive sensitivity gives the relative magnitude of the contribution of that discrete point in the domain to the overall noise field, assuming $\langle |\sigma(x_0,y_0)|^2 \rangle$ is uniform everywhere. Though this is the case for wind driven noise, for spatially non-uniform noise processes such as a rain storm the transmission loss must be computed using the source strength modulated pressure field given by

$$\mathrm{TL} = 10 \log \left\{ \langle |\sigma(x_0,y_0)|^2 \rangle p_1(\omega,x_i,y_j,z') \right\}. \tag{28}$$

Values of the ensemble average of the noise source strength for wind driven breaking waves have been empirically derived and experimentally measured (Burgess and Kewley, 1983; Kuperman and Ferla, 1985; Farmer and Vagle, 1988; Kewley *et al.*, 1990). In this study we are primarily concerned with the coherence of uniformly distributed noise sources, which is not dependent on source spectrum or level.

Computationally, we can relate the surface noise level distribution at each discrete point to the total noise probability distribution function. First, we assume the noise at each discrete point in the domain is the summation of several wave-breaking events, which by the central limit theorem yields a Gaussian source distribution. This is realistic since each point represents an area on the order 10^2 m^2 for a typical order wavelength PE range step. This is further compounded by the fact that the mean noise level predicted here is an ensemble averaged level due to a stationary process. In other words, the measurement was taken over some average in time greater than time scales of the individual breaking wave, yet, less than the time scale of a change in wind stress or mean wave height. Thus, the ensemble of breaking waves at each discrete point in the domain can be modeled as a

single source with amplitude determined by a Gaussian distribution

$$\langle |\sigma(x_i, y_j)|^2 \rangle = f_x(Q) = \frac{1}{\sigma\sqrt{2\pi}} e^{-(Q-\mu)^2/2\sigma^2}, \tag{29}$$

where μ is the mean, σ is standard deviation, and Q is the random variable representing the source level of a single wave breaking event. The numerical values of these coefficients and their relationships to meteorological and oceanographic processes and forcing are beyond the scope of the work presented in this paper.

Since the noise level of each ensemble averaged source is a function of a random variable Q, we can calculate the total mean noise level distribution by examining Eq. (26). It shows that the total noise is simply a sum of each individual ensemble averaged noise source receive level, weighted by the product of the source's amplitude, given by Eq. (29), and the elemental area over which the source has been averaged.

2. Benchmark: Vertical noise coherence in a Pekeris waveguide

The noise coherence is an integral over phase differences between two closely spaced sensors as a function of range. For this reason, the size of the range stepping is akin to a spatial sampling frequency. If the sampling frequency is too low, the integrand is too poorly sampled and the error on the integral, the mean noise level, is large. As the frequency increases, the integrand varies more quickly with range, therefore, the range step size must be decreased relative to the wavelength in order to maintain constant uncertainty on the coherence. In order to verify the accuracy of the reciprocal PE model and determine the required range and depth grid spacing, the vertical noise coherence in a shallow water Pekeris waveguide was calculated and compared to the analytical solution (Deane *et al.*, 1997). A non-uniform depth grid spacing was used, allowing the depth of the noise sources below the surface to be placed arbitrarily without increasing computational cost. The monopole noise sources were placed at 8.5 cm for all frequencies in both the PE model and the waveguide integral full field solution as specified by Deane *et al.* (1997). The comparison of the full field solution and PE modeled solution of the real and imaginary vertical noise coherence plotted against dimensionless frequency $\bar{\omega} = \omega d/c$ is shown in Fig. 2, where d is the sensor spacing and c is 1500 m/s, the sound speed in a Pekeris waveguide with a depth of 50 m, bottom sound speed of 1650 m/s, and bottom density of 1700 kg/m^3. The fit between the two models is reasonable with some error in the PE modeled coherence at low dimensionless frequency due to a combination of limited spatial resolution in depth and range, and the inability of the PE model to propagate energy at angles steeper than ~89 deg. These errors combine at each frequency step cumulatively and with different magnitudes depending on frequency, leading to a jagged estimate of coherence.

3. Horizontal coherence and directionality

The horizontal coherence cannot be calculated directly from the reciprocity PE model in the cylindrical coordinate system, since the receiver must always be placed at the origin. A second horizontally displaced receiver would involve defining a new coordinate origin, making the computation of the complex pressure field along the radials in the original coordinate system difficult; the two co-located fields are a requirement for computing the reciprocal cross-spectral and power spectral densities.

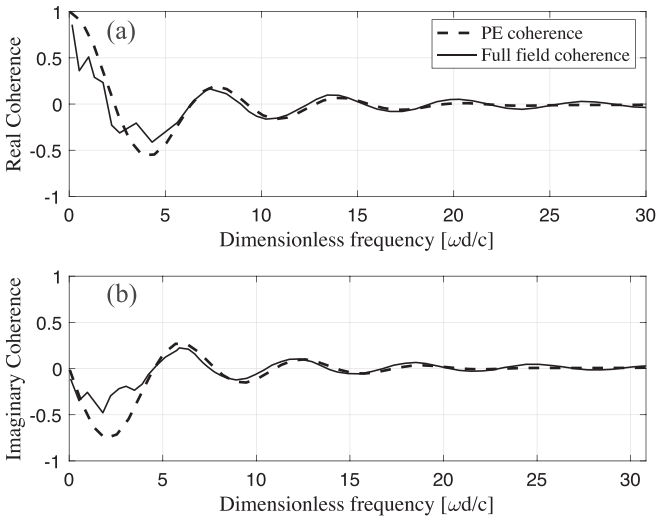

FIG. 2. (a) Real and (b) imaginary components of the vertical noise coherence in a Pekeris waveguide, calculated by the PE reciprocity method (solid lines) and the exact wave number integral solution (dashed lines).

However, ambient noise in the ocean can be modeled by a superposition of plane waves, and the horizontal noise directionality can be used to compute the horizontal noise coherence, using the relationship derived by Cox (1973),

$$\Gamma(\bar{\omega}) = \frac{1}{2}\int_0^{\pi} F(\theta) e^{-i\bar{\omega}\cos\theta} \sin\theta \, d\theta, \tag{30}$$

where $F(\theta)$ is the directional density function in the horizontal case, θ is the angle of azimuth, and Γ is the noise coherence between two sensors, or the normalized cross-spectral density,

$$\Gamma_{12} = \frac{S_{12}}{\sqrt{S_{11}S_{22}}}. \tag{31}$$

For the familiar case of isotropic noise, the coherence is given by $\Gamma(\bar{\omega}) = \mathrm{sync}(\bar{\omega})$, with the familiar zero crossings at $\lambda/2$. More general closed form relationships between horizontal coherence and directionality have been described by Walker and Buckingham (2012).

The horizontal noise directionality can be directly computed from the computational noise models by integrating along each bearing of surface receive sensitivity. This is straightforward in the Nx2D case. In the cylindrical 3D case, since the grid spacing employed by the PE marching scheme is non-uniform in range, the domain is divided into one-degree wedges, with all the contributing noise sources within each wedge summing to the total noise received at that angle. The contributing area for each noise source must be carefully accounted for since the cylindrical elemental areas are of the form $r\Delta r\Delta\theta(r)$, where the azimuthal differential $\Delta\theta$ varies in

range due to the azimuthal grid upsampling method employed in the marching algorithm (Lin *et al.*, 2012).

III. RESULTS AND DISCUSSION

A. Normal modes

To arrive at the noise cross or power spectrum using the normal mode method, we must first compute the mode shapes and then combine them with the cross modal amplitudes shown in Fig. 1. For a Gaussian canyon with $C = 100$ m and $B = 50$ m, and a fluid bottom half-space with a sound speed of 1700 m/s and a density of 1700 kg/m^3, the across-canyon dependencies of the vertical wave number for the first five vertical modes are shown in Fig. 3. The resulting modes shapes for the canyon bathymetry plotted in Fig. 3(a) are shown for the first five across-canyon horizontal modes of the first six vertical modes in Fig. 4, showing the relationship between the vertical modes, vertical wave number, and horizontal mode shapes.

The computed horizontal mode shapes can then be substituted into the approximate expression for noise cross-spectral density and power-spectral density given by Eq. (19). As Eq. (31) shows, the noise coherence is independent of the frequency characteristics of the ensemble average of source terms $\langle|\sigma(x_0, y_0)|^2\rangle$ shown as a multiplicative factor outside of the quadruple sum in Eq. (19). The real component of the vertical coherence calculated using the first 10 horizontal modes for each of the first 16 vertical modes is shown in Fig. 5.

The computation of the cross modal amplitudes for the cross-spectral and power-spectral densities for two receivers placed in the y-z plane may be simplified by neglecting all terms except those that satisfy $n = n'$ and $m = m'$. Figure 5 compares the real component of the vertical coherence for the full mode sum versus the simplified sum. The two curves are in good agreement, with their zero crossings nearly identical, showing that the excluded modes are not large contributors to the noise coherence as predicted by the expression for the cross modal amplitudes in Eq. (19).

Although the solution is robust to the exclusion of cross modes, the normal mode solution does not include mode coupling. In certain 2D and 3D environments, mode coupling can be critical for computing an accurate sound field (Ballard *et al.*, 2015). PE propagation models can avoid this problem, and thus provide an attractive alternative for 3D noise modeling.

B. Nx2D and cylindrical 3D PE

The vertical coherence was calculated using the reciprocity PE method between two sensors placed at 50 m depth in the center of a North–South oriented Gaussian canyon with a maximum depth of 100 m. A 2D PE model run was carried out for a source at 50 and 51 m, at every one degree of bearing, creating an Nx2D version of the surface receive sensitivity. The surface receive sensitivity for noise at 750 Hz on the receiver at 50 m depth is shown in Fig. 6(a). The bathymetric effect increases the noise sensitivity along the canyon axis relative to bearings across the canyon, even without the effect of horizontal reflection or refraction. Indeed, such a bathymetric shadowing effect has been observed in deep ocean trenches (Barclay and Buckingham, 2014).

In order to capture the effects of horizontal reflection and refraction of noise due to the canyon's bathymetry, a cylindrical 3D PE model must be employed (Lin *et al.*, 2012; Lin *et al.*, 2013a). The surface receive sensitivity for a receiver placed at 50 m depth in a Gaussian canyon as previously described at 750 Hz shows increased noise sensitivity along the canyon axis, shown in Fig. 6(b). When compared to the Nx2D case with the identical geometry and model properties, it is apparent that the trapped horizontal modes in

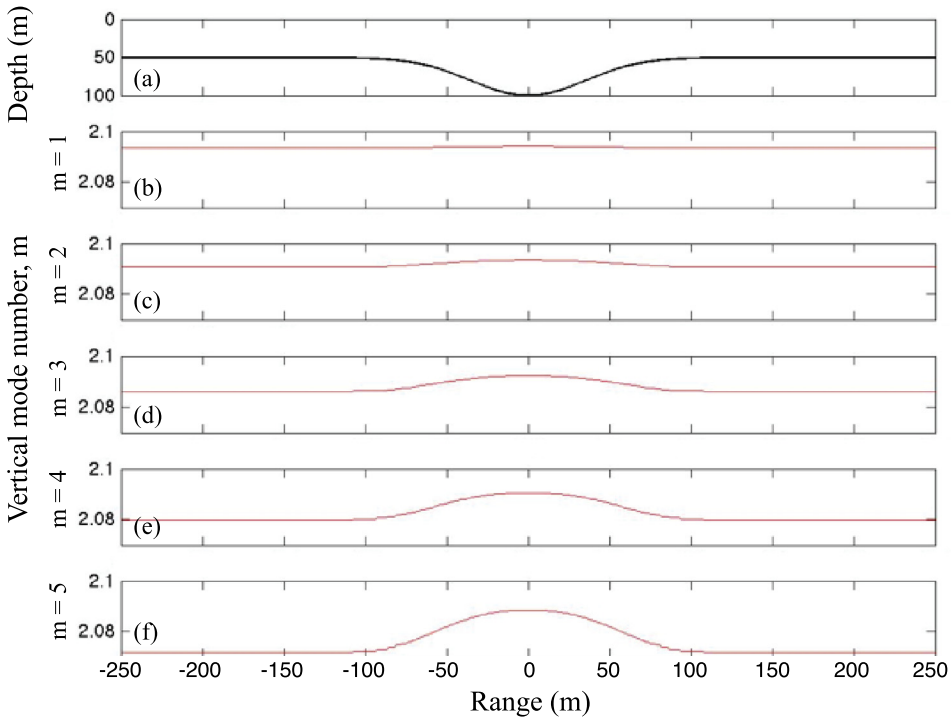

FIG. 3. (Color online) Vertical wave number as a function of across-canyon range, where the bathymetry is given in (a), for the first five vertical modes (b)–(f), indexed by m, at 500 Hz.

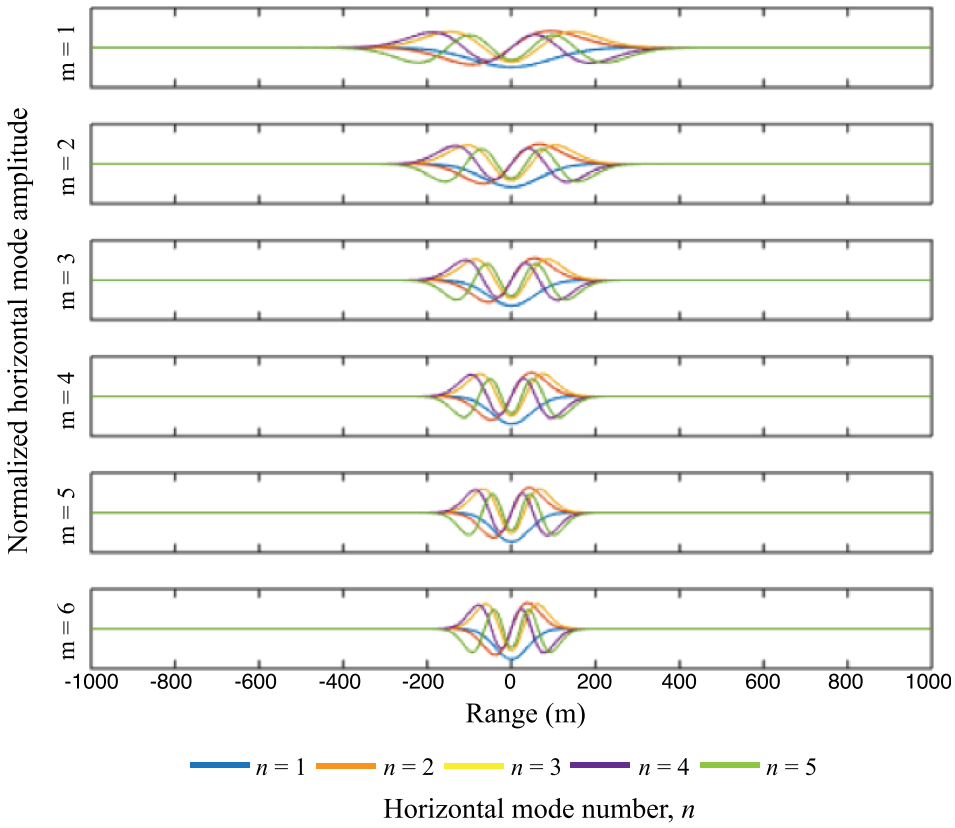

FIG. 4. (Color online) The first five horizontal mode shapes with mode number, n, for each of the first six vertical modes, m, for the Gaussian canyon bathymetry from Fig. 3(a) at 500 Hz. Note the increase in range scale.

the canyon play an important role in shaping the horizontal directionality of the noise field. Noise sources at ranges greater than 500 m, at mid-quadrant azimuthal angles (e.g., 45 deg, 135 deg, etc.) contribute less to the total noise field when compared to the Nx2D case. In the non-reciprocal picture, the effect of the out-of-plane component of the seafloor reflection and horizontal refraction on sound propagating out of the canyon causes a focusing along the axis, and thus a reduction of sound reaching the mid-quadrant regions.

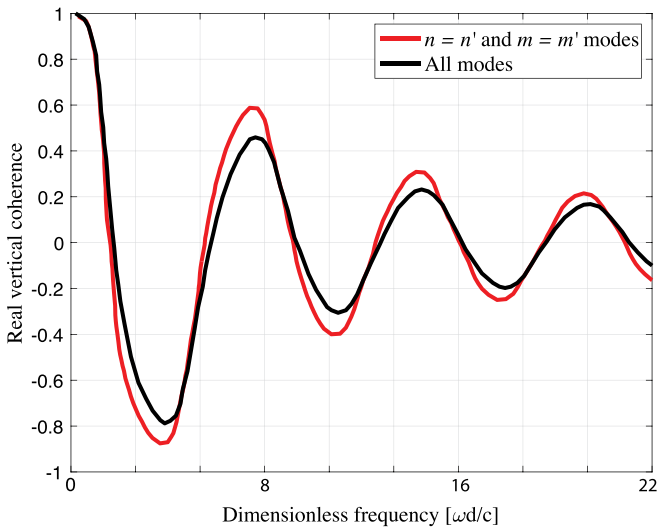

FIG. 5. (Color online) Comparison of the real component of the vertical noise coherence calculated with the full mode sum (black line) and simplified modal sum, in which only the modes where $n = n'$ and $m = m'$ are kept (red line) for two receivers centered at 50 m over the axis of the Gaussian canyon shown in Fig. 3(a).

For both the Nx2D and 3D cases, the surface receive sensitivity shows an across–along-canyon asymmetry in the relative noise field contributions over short (<500 m) ranges. In the Nx2D case, any asymmetry between the across- and along-canyon directions in the noise field due to nearby sources (<500 m away) is largely outweighed by the angularly uniform contributions from more distant sources, shown in the nearly isotropic horizontal noise directionality in Fig. 7(a). This is due to the fact that although the distant sources are weaker in amplitude, their total contribution is multiplied by the cylindrical coordinate element of area, hence, scaling linearly with range from the receiver. This effect places more importance on the distant contributions of surface noise to the overall field and, hence, masks the effect of the canyon on the horizontal noise directionality.

Figure 7(b) presents the horizontal directionality showing a pronounced increase in noise arriving along the trench axis (90 and 270 deg), with a lower noise contribution arriving from other bearings. Distant sources do not reach the receiver with the same intensity that they do in the Nx2D case because of the out-of-plane propagation. Instead, we see increased focusing of noise along traveling along the axis, while distance mid-quadrant sources do not reach the receiver.

The vertical coherence can be directly calculated using the reciprocal PE method. Figures 8(a) and 8(b) show the real and imaginary components of the vertical coherence computed using the Nx2D for noise arriving from along (90 deg bearing angle) and across (0 deg bearing angle) canyon axis directions. Figures 8(c) and 8(d) show the same results computed using the 3D PE method. A conventional hydrophone with omnidirectional sensitivity would record the mean of these two curves along with all the contributions

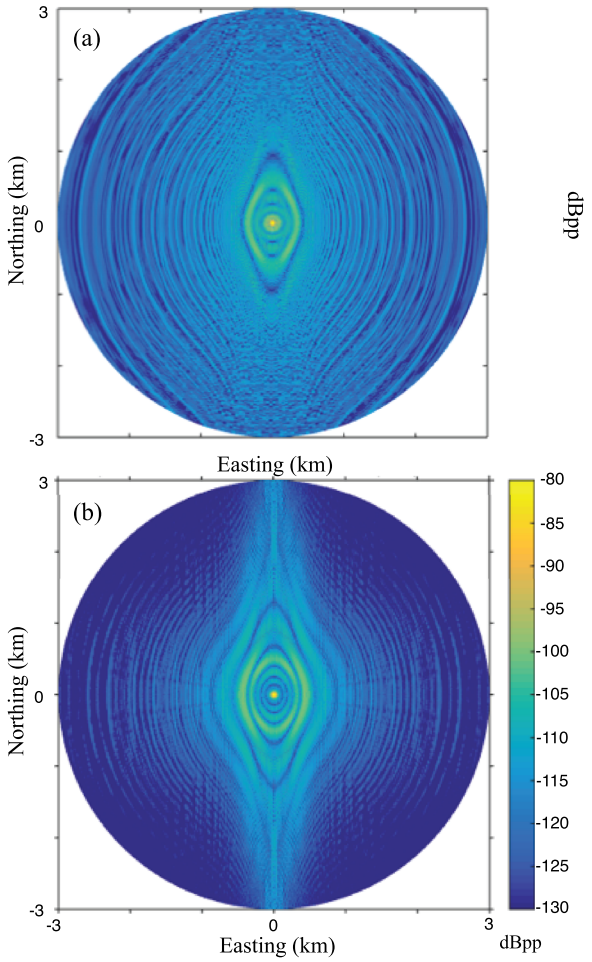

FIG. 6. (Color online) (a) Nx2D and (b) cylindrical 3D PE calculated surface receive sensitivities at 0.1 m, 750 Hz for a receiver placed at 50 m depth over the center of a Gaussian canyon with bathymetry shown in Fig. 3(a) and the axis oriented North–South.

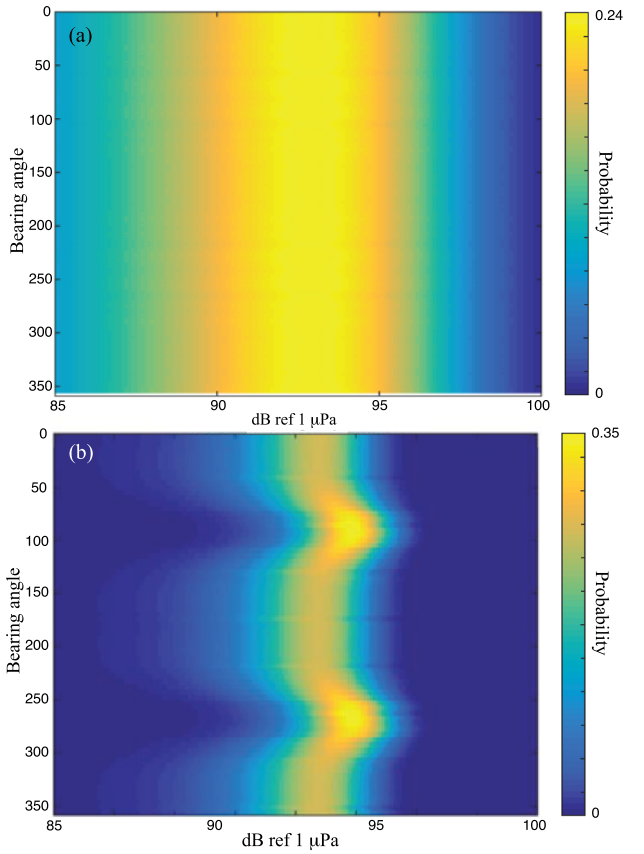

FIG. 7. (Color online) Probability distribution function of noise as a function of bearing (arrival) angle predicted by the (a) Nx2D and (b) cylindrical 3D PE noise model at 750 Hz for a receiver placed at 50 m in the center of a Gaussian canyon with a bathymetry shown in Fig. 3(a) and the axis oriented North–South (90–270 deg bearing).

from the other bearing angles. Using the PE reciprocity method, the vertical noise coherence contribution from a chosen bearing angle can be calculated individually. The small displacement of the zero crossings and mismatch between the curves shows in both models that the noise coherence is influenced by bathymetric shadowing. A comparison of the Nx2D and 3D vertical noise coherences shows the zero crossing in the real component to be significantly shifted, demonstrating the importance of horizontal refraction and reflection in modeling the noise near a submarine canyon.

C. Inter-model comparison

The real vertical noise coherence at a depth of 50 m over a 100 m deep Gaussian canyon with bathymetry shown in Fig. 3(a) is calculated using the normal mode quasi-analytical model and the 3D PE computational model, and compared in Fig. 9. Both models have isovelocity sound speed profiles and typical parameters for a hard sandy bottom. The adiabatic approximation and the fact that the normal mode model only describes the across-canyon sound field, which can be expressed as horizontal trapped modes, explains some of the misfit between the two models. Although the form and oscillatory behavior is replicated by both models, the zero crossings and amplitudes are not well matched.

IV. HUDSON CANYON EXAMPLE

By comparing the Nx2D and cylindrical 3D PE noise models in a realistic ocean environment, the effects of horizontal reflection and refraction on the mean noise level, horizontal directionality, and vertical coherence can be shown. As an example, a simulated receiver is placed at 50 m depth along the axis of the Hudson Canyon, shown in Fig. 10(top), with an isovelocity sound speed profile, and a uniform half-space seabed with compressional sound speed 1700 m/s and a density of 1700 kg/m^3 is simulated.

The vertical coherence for four bearing angles, 0 and 180 deg, the approximate across-canyon directions, and 55 and 285 deg up and down the canyon axis, are shown in Figs. 10(a), 10(b), 10(c), and 10(d), respectively. The Nx2D and cylindrical 3D results are intercompared and plotted versus dimensionless frequency. The Cron and Sherman vertical coherence model is plotted as a visual reference for a deep-water environment with no bathymetric influence on the noise field. In the two across-canyon directions both computational models agree. Noise propagating across the canyon propagates within the vertical plane. The mismatch between the PE modeled results and the Cron and Sherman model for

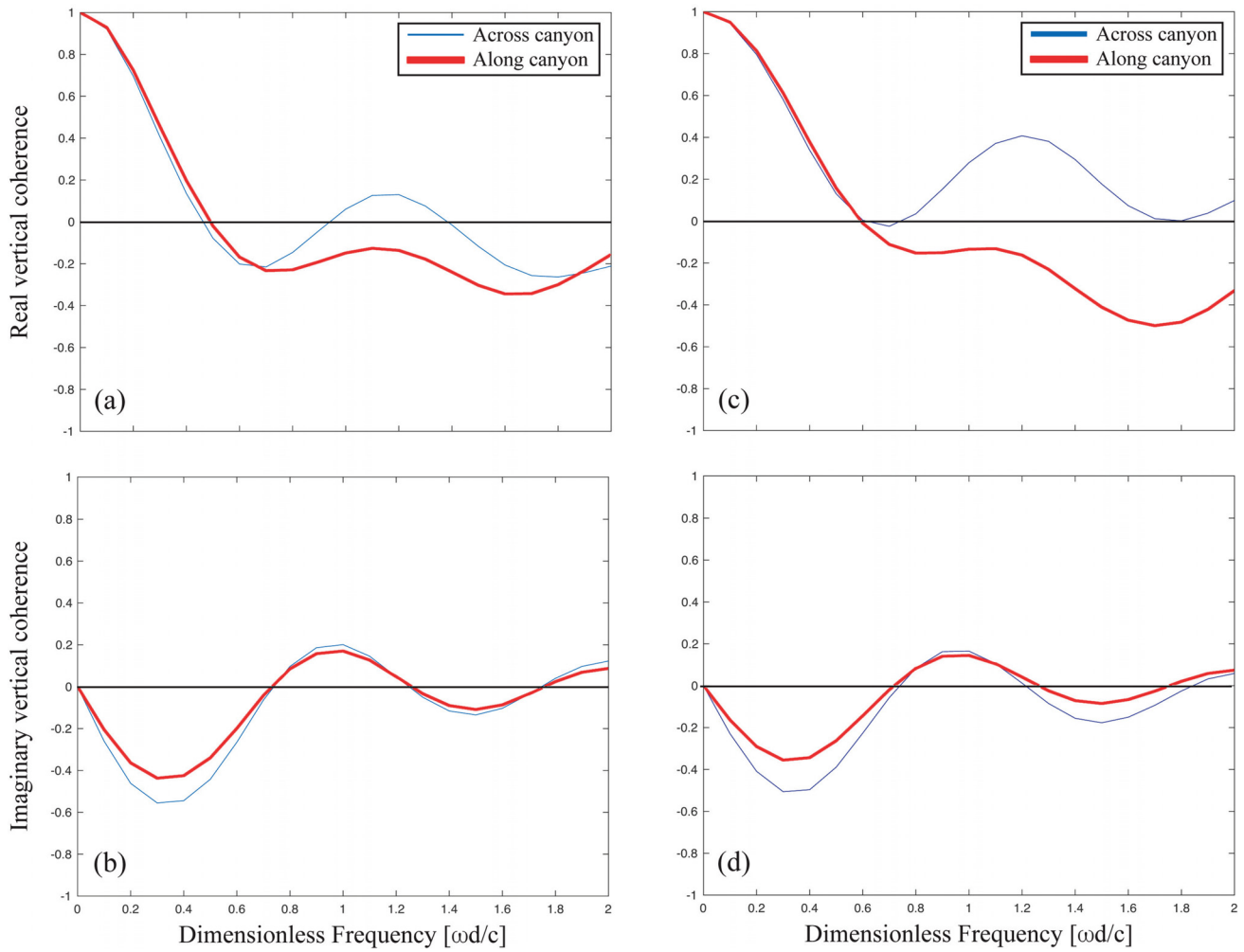

FIG. 8. (Color online) (a) Real and (b) imaginary components of the vertical coherence of noise arriving from along (thick red line) and across (thin blue line) the canyon axis, calculated using Nx2D PE, and (c) real and (d) imaginary components of the vertical coherence of noise calculated using 3D cylindrical PE.

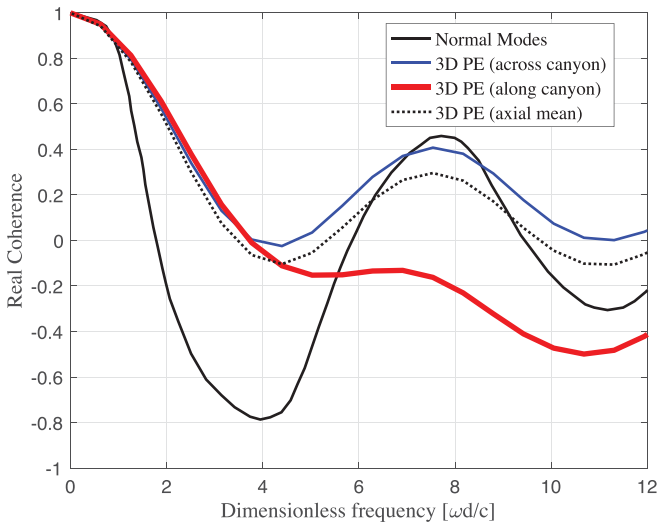

FIG. 9. (Color online) The real vertical noise coherence for a pair of receivers placed at 50 m depth over the axis of a Gaussian canyon, shown in Fig. 3(a), calculated using the normal mode model (solid black line) and 3D cylindrical PE model for noise arriving from the across-canyon direction (thin blue line), along-canyon direction (thick red line), and at all axial angles (dashed black line).

noise in an infinite half-space (i.e., bottomless ocean) shows the in-plane effect of the bathymetry on vertical noise coherence. However, for noise propagating along the canyon axis in either direction, 3D effects become apparent. Focusing of the noise field along the axis by horizontal reflections shifts the zero crossings of the coherence, and increases the absolute coherence a higher dimensionless frequency. This effect is larger for noise arriving from the shallower and narrower canyon head, relative to noise arriving from the deeper and wider canyon mouth.

V. CONCLUSIONS

A quasi-analytical 3D adiabatic normal mode model (neglecting mode coupling) for longitudinally invariant environments can be used to quickly compute vertical noise coherence curves in idealized ocean environments. An examination of the cross modal amplitudes in the modal decomposition of the noise cross-spectral density shows that the computation can be simplified, without loss of fidelity, by modifying the vertical and horizontal mode sums to exclude non-identical mode numbers. This holds for all longitudinally invariant 3D environments, and was demonstrated for the particular case of an infinitely long Gaussian

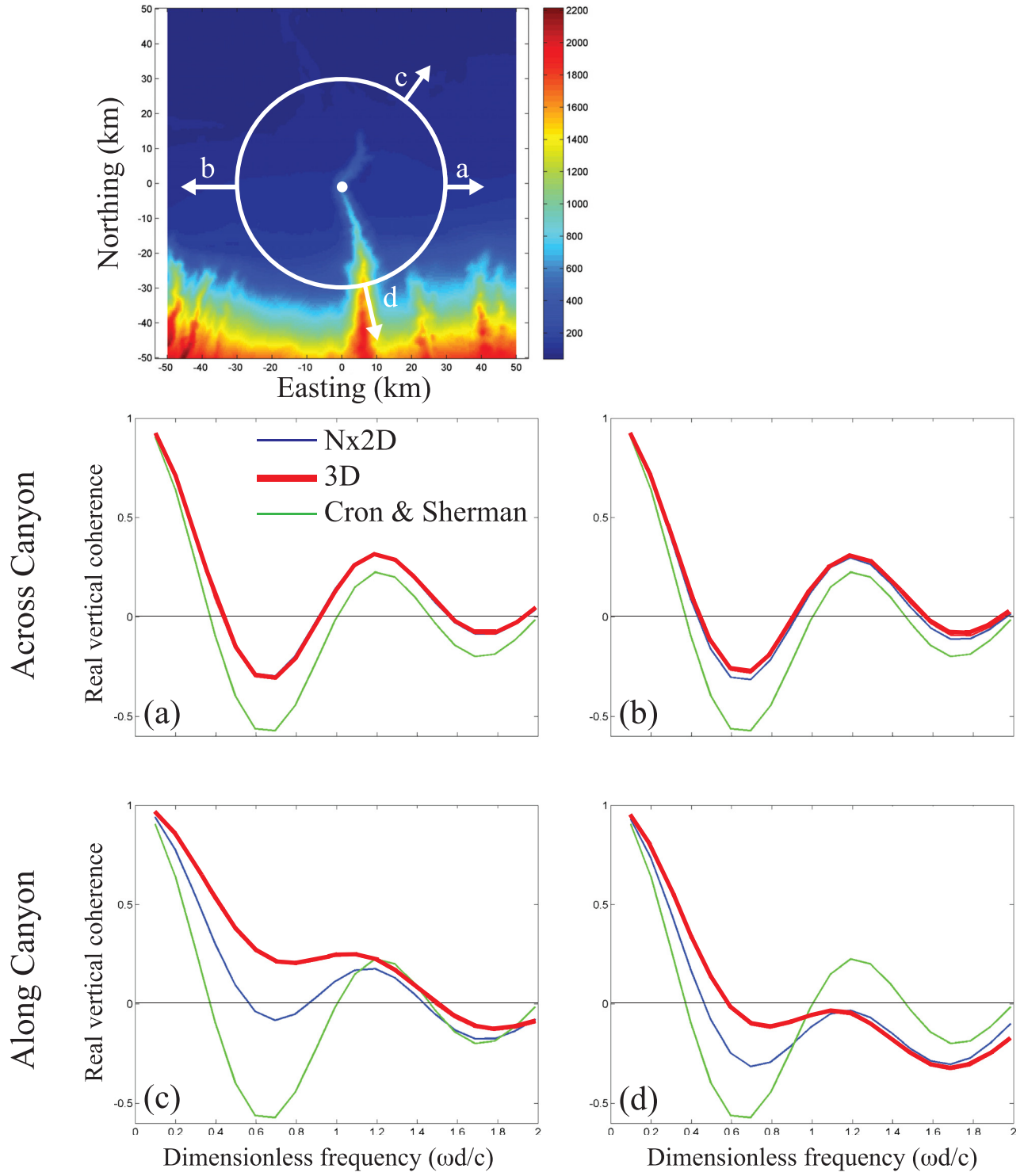

FIG. 10. (Color online) Bathymetry of Hudson Canyon (top) with the receiver location (white dot) and bearings along which the real component of the vertical coherence was calculated using the Nx2D model (thin blue line) and cylindrical 3D model (thick red line) across the canyon at (a) 0 deg, (b) 180 deg, and along the canyon axis at (c) 55 deg and (d) 285 deg. The Cron and Sherman model for deep water vertical noise coherence (light green line) is plotted for comparison.

canyon, where it was seen that the across-canyon variation of the vertical wave number associated with each mode allows a set of horizontally trapped modes to be generated.

Additionally, to take into account the acoustic mode coupling, two PE reciprocity noise modeling methods were used to compute the horizontal noise probability distribution directionality, surface receive sensitivity, and vertical noise coherence for a receiver placed at the center of a Gaussian canyon. The first used a standard Nx2D PE propagation code, while the second used a cylindrical 3D PE propagation code, capable of resolving horizontal reflections from the seabed and horizontal refraction. The 3D propagation effects were shown to significantly affect the noise field by focusing sound that propagates along the axis of the canyon, thus amplifying the contribution of noise arriving from the up and down axes directions. This effect can be seen in the surface receive sensitivity and horizontal noise directionality. Additionally, these 3D propagation effects alter the zero

crossings of the vertical coherence. Noise arriving from directions both along and across the canyon's axis shows increased absolute coherence. This increase is due to a larger contribution from the real component, which represents noise whose directional density function is symmetric about the horizontal, while the imaginary component, which represents noise whose directional density function is antisymmetric about the horizontal, shows no change when 3D effects are included. The additional noise, which is focused by horizontal reflections from the canyon's bathymetry, propagates as a set of trapped horizontal and vertical modes, and thus contributes to the noise directional density symmetrically. The adiabatic and trapped horizontal mode approximations made in the development of the normal mode model cause significant degradation of vertical coherence predictions, when compared with the cylindrical 3D PE model. To correctly model the vertical coherence in a submarine canyon, a full 3D computational model is required.

This last effect was demonstrated by simulation in a realistic ocean environment, the Hudson Canyon, a shelf break submarine canyon located off the coast of New Jersey. It was found that the focusing effect of the canyon on the vertical noise coherence is significant in the along axis directions of the canyon, particularly for noise arriving from the shallower, narrower head of the canyon. In order to develop more sophisticated and effective sensor arrays, signal processing algorithms, and acoustical oceanographic sensing methods for use in regions near shelf break canyons, these 3D effects must be included in noise model predictions.

ACKNOWLEDGMENTS

The authors wish to acknowledge Arthur Newhall for his technical support. This work was supported by the Office of Naval Research, Ocean Acoustic Code 322OA, under Grant Nos. N00014-15-1-2629 and N00014-17-1-2692, and by the Natural Sciences and Engineering Research Council of Canada's Research Chair, and Discovery Grant program.

Ballard, M. S., Goldsberry, B. M., and Isakson, M. J. (**2015**). "Normal mode analysis of three-dimensional propagation over a small-slope cosine shaped hill," J. Comp. Acoust. **23**, 1550005.

Ballard, M. S., Lin, Y.-T., and Lynch, J. F. (**2012**). "Horizontal refraction of propagating sound due to seafloor scours over a range-dependent layered bottom on the New Jersey shelf," J. Acoust. Soc. Am. **131**, 2587–2598.

Barclay, D. R., and Buckingham, M. J. (**2013**). "Depth dependence of wind-driven, broadband ambient noise in the Philippine Sea," J. Acoust. Soc. Am. **133**, 62–71.

Barclay, D. R., and Buckingham, M. J. (**2014**). "On the spatial properties of ambient noise in the Tonga Trench, including effects of bathymetric shadowing," J. Acoust. Soc. Am. **136**, 2497–2511.

Buckingham, M. J. (**1979**). "Array gain of a broadside vertical linear array in shallow water," J. Acoust. Soc. Am. **65**, 148–161.

Buckingham, M. J. (**1994**). "On surface-generated ambient noise in an upward refracting ocean," Proc. R. Soc. London, Ser. A **346**, 321–352.

Burgess, A., and Kewley, D. (**1983**). "Wind-generated surface noise source levels in deep water east of Australia," J. Acoust. Soc. Am. **73**, 201–210.

Carbone, N. M., Deane, G. B., and Buckingham, M. J. (**1998**). "Estimating the compressional and shear wave speeds of a shallow water seabed from the vertical coherence of ambient noise in the water column," J. Acoust. Soc. Am. **103**, 801–813.

Carey, W. M., and Evans, R. B. (**2011**). *Ocean Ambient Noise: Measurement and Theory* (Springer Science and Business Media, New York).

Carey, W. M., Evans, R. B., Davis, J. A., and Botseas, G. (**1990**). "Deep-ocean vertical noise directionality," IEEE J. Oceanic Eng. **15**, 324–334.

Cox, H. (**1973**). "Spatial correlation in arbitrary noise fields with application to ambient sea noise," J. Acoust. Soc. Am. **54**, 1289–1301.

Cron, B. F., and Sherman, C. H. (**1962**). "Spatial-correlation functions for various noise models," J. Acoust. Soc. Am. **34**, 1732–1736.

Deane, G. B., Buckingham, M. J., and Tindle, C. T. (**1997**). "Vertical coherence of ambient noise in shallow water overlying a fluid seabed," J. Acoust. Soc. Am. **102**, 3413–3424.

Dyer, I. (**1973**). "Statistics of distant shipping noise," J. Acoust. Soc. Am. **53**, 564–570.

Farmer, D. M., and Vagle, S. (**1988**). "On the determination of breaking surface wave distributions using ambient sound," J. Geophys. Res. **93**, 3591–3600, https://doi.org/10.1029/JC093iC04p03591.

Glegg, S. A., and Yoon, J. R. (**1990**). "Experimental measurements of three-dimensional propagation in a wedge-shaped ocean with pressure-release boundary conditions," J. Acoust. Soc. Am. **87**, 101–105.

Heaney, K. D., and Murray, J. J. (**2009**). "Measurements of three-dimensional propagation in a continental shelf environment," J. Acoust. Soc. Am. **125**, 1394–1402.

Jensen, F. B. (**1994**). *Computational Ocean Acoustics* (American Institute of Physics, Melville, NY).

Kewley, D., Browning, D., and Carey, W. (**1990**). "Low-frequency wind-generated ambient noise source levels," J. Acoust. Soc. Am. **88**, 1894–1902.

Kuperman, W., and Ferla, M. (**1985**). "A shallow water experiment to determine the source spectrum level of wind-generated noise," J. Acoust. Soc. Am. **77**, 2067–2073.

Kuperman, W. A., and Ingenito, F. (**1980**). "Spatial correlation of surface generated noise in a stratified ocean," J. Acoust. Soc. Am. **67**, 1988–1996.

Lin, Y.-T., Collis, J. M., and Duda, T. F. (**2012**). "A three-dimensional parabolic equation model of sound propagation using higher-order operator splitting and Padé approximants," J. Acoust. Soc. Am. **132**, EL364–EL370.

Lin, Y.-T., Duda, T. F., Emerson, C., Gawarkiewicz, G., Newhall, A. E., Calder, B., Lynch, J. F., Abbot, P., Yang, Y.-J., and Jan, S. (**2015**). "Experimental and numerical studies of sound propagation over a submarine canyon northeast of Taiwan," IEEE J. Oceanic Eng. **40**, 237–249.

Lin, Y.-T., Duda, T. F., and Newhall, A. E. (**2013a**). "Three-dimensional sound propagation models using the parabolic-equation approximation and the split-step Fourier method," J. Comp. Acoust. **21**, 1250018.

Lin, Y.-T., and Lynch, J. F. (**2012**). "Analytical study of the horizontal ducting of sound by an oceanic front over a slope," J. Acoust. Soc. Am. **131**, EL1–EL7.

Lin, Y.-T., McMahon, K. G., Lynch, J. F., and Siegmann, W. L. (**2013b**). "Horizontal ducting of sound by curved nonlinear internal gravity waves in the continental shelf areas," J. Acoust. Soc. Am. **133**, 37–49.

Perkins, J. S., Kuperman, W., Ingenito, F., Fialkowski, L. T., and Glattetre, J. (**1993**). "Modeling ambient noise in three-dimensional ocean environments," J. Acoust. Soc. Am. **93**, 739–752.

Perkins, J. S., and Thorsos, E. I. (**2007**). "Overview of the reverberation modeling workshops," J. Acoust. Soc. Am. **122**, 3074.

Sagers, J. D., Ballard, M. S., and Knobles, D. P. (**2014**). "Evidence of three-dimensional acoustic propagation in the Catoche Tongue," J. Acoust. Soc. Am. **136**, 2453–2462.

Siderius, M., Harrison, C. H., and Porter, M. B. (**2006**). "A passive fathometer technique for imaging seabed layering using ambient noise," J. Acoust. Soc. Am. **120**, 1315–1323.

Vagle, S., Large, W. G., and Farmer, D. M. (**1990**). "An evaluation of the WOTAN technique of inferring oceanic winds from underwater ambient sound," J. Atmos. Ocean. Tech. **7**, 576–595.

Walker, S. C., and Buckingham, M. J. (**2012**). "Spatial coherence and cross correlation of three-dimensional ambient noise fields in the ocean," J. Acoust. Soc. Am. **131**, 1079–1086.

Weston, D. E. (**1960**). "A Moiré fringe analog of sound propagation in shallow water," J. Acoust. Soc. Am. **32**, 647–654.

Westwood, E. K., Tindle, C. T., and Chapman, N. R. (**1996**). "A normal mode model for acousto-elastic ocean environments," J. Acoust. Soc. Am. **100**, 3631–3645.